Focal mechanisms produced by shear faulting in weakly transversely isotropic crustal rocks

Václav Vavryčuk[1]

ABSTRACT

Shear faulting in anisotropic rocks produces non-double-couple (non-DC) mechanisms. The non-DC mechanisms can comprise the isotropic (ISO) and compensated linear vector dipole (CLVD) components. The formulas for percentages of the ISO and CLVD are simplified under the assumption of weak transverse isotropy and can be expressed advantageously in terms of Thomsen's anisotropy parameters. Shear faulting in crustal rocks with anisotropy strength of 10% can produce an ISO of up to 10% and a CLVD of up to 30%. Such values are significant and detectable in carefully determined focal mechanisms.

INTRODUCTION

Focal mechanisms of earthquakes provide valuable information about the orientation of fractures, type of faulting, pore pressure, and tectonic stress in a seismically active area. In exploration geophysics, focal mechanisms can be determined for microearthquakes induced in reservoirs during gas or oil production or during well stimulation by hydraulic fracturing (Rutledge and Phillips, 2003). Knowledge of focal mechanisms helps enhance reservoir characterization by imaging the orientation, complexity, and temporal growth of induced fractures and by fault mapping (Rutledge et al., 1998; Maxwell and Urbancic, 2001). Focal mechanisms can be utilized also in estimating pore pressure. If pore pressure is low, only shear faulting is observed and focal mechanisms are double couple (DC). If pore pressure is high, tensile faulting is observed and focal mechanisms are non-DC (Vavryčuk, 2001, 2002).

So far, focal mechanisms have been mainly computed and interpreted under the assumption of an isotropic medium. The geologic structures of the earth's crust, however, frequently display anisotropy (Thomsen, 1986; Babuška and Cara, 1991; Tsvankin, 2001), which can be caused by sediment layering; by the presence of aligned microcracks, cracks, or fractures; or by the textural ordering of rock-forming minerals. Anisotropy not only significantly influences seismic wave propagation (Musgrave, 1970; Kravtsov and Orlov, 1990; Helbig, 1994; Červený, 2001), but it also alters and complicates the properties of seismic sources (Kawasaki and Tanimoto, 1981; Julian et al., 1998; Rössler et al., 2004; Vavryčuk, 2004). For example, Vavryčuk (2005) has shown that DC mechanisms produced by shear faulting under isotropy can become non-DC under anisotropy. Also the fault-plane solutions calculated under the assumption of isotropy can deviate from the true orientations if the source area is actually anisotropic (Šílený and Vavryčuk, 2002).

In this paper, I continue earlier work (Vavryčuk, 2005) in which focal mechanisms in general anisotropy of arbitrary symmetry and arbitrary strength are studied. I specify this theory for weak transverse isotropy, the most commonly assumed type of anisotropy used in exploration geophysics. Applying the first-order perturbation theory (Pšenčík and Gajewski, 1998; Vavryčuk and Pšenčík, 1998; Pšenčík and Dellinger, 2001; Farra, 2004, 2005), I derive approximate formulas for the non-DC components produced by shear faulting in transversely isotropic (TI) media. The formulas are expressed using Thomsen's anisotropy parameters (Thomsen, 1986; Tsvankin and Thomsen, 1994), and accuracy of the derived approximations is tested on theoretical models of crustal anisotropy as well as anisotropy observed in crustal rock samples.

MOMENT TENSORS IN ANISOTROPIC MEDIA

The moment tensor $\mathbf{M}$ of a seismic source situated in an anisotropic medium is expressed as (Vavryčuk, 2005, equation 4)

$$M_{ij} = c_{ijkl}D_{kl}. \tag{1}$$

Tensor c_{ijkl} is the tensor of elastic parameters of the anisotropic medium surrounding the fault, and tensor D_{kl} denotes the seismic source tensor

$$D_{kl} = \frac{uS}{2}(\nu_k n_l + \nu_l n_k), \tag{2}$$

where u is the slip, S the fault area, $\boldsymbol{\nu}$ the slip direction, and $\mathbf{n}$ the fault normal. If vectors $\boldsymbol{\nu}$ and $\mathbf{n}$ are perpendicular, the source tensor de-

scribes shear faulting; if they are arbitrarily oriented, the source tensor describes tensile faulting.

In general, the moment tensors in anisotropic media are complicated. They can be decomposed into the DC, compensated linear vector dipole (CLVD), and isotropic (ISO) parts

$$\mathbf{M} = \mathbf{M}^{\mathrm{ISO}} + \mathbf{M}^{\mathrm{CLVD}} + \mathbf{M}^{\mathrm{DC}}, \tag{3}$$

which are defined as follows (Jost and Hermann, 1989; Vavryčuk, 2005):

$$\mathbf{M}^{\mathrm{ISO}} = \frac{1}{3}\mathrm{Tr}(\mathbf{M})\begin{bmatrix} 1 & 0 & 0 \\ 0 & 1 & 0 \\ 0 & 0 & 1 \end{bmatrix}, \tag{4}$$

$$\mathbf{M}^{\mathrm{CLVD}} = |\varepsilon^{\mathrm{CLVD}}|M^*_{|\mathrm{max}|}\begin{bmatrix} -1 & 0 & 0 \\ 0 & -1 & 0 \\ 0 & 0 & 2 \end{bmatrix}, \tag{5}$$

$$\mathbf{M}^{\mathrm{DC}} = (1 - 2|\varepsilon^{\mathrm{CLVD}}|)M^*_{|\mathrm{max}|}\begin{bmatrix} -1 & 0 & 0 \\ 0 & 0 & 0 \\ 0 & 0 & 1 \end{bmatrix}, \tag{6}$$

where $\mathrm{Tr}(\mathbf{M})$ is the trace of tensor $\mathbf{M}$. Parameter $\varepsilon^{\mathrm{CLVD}}$ measures the size of the CLVD relative to the DC and is defined as

$$\varepsilon^{\mathrm{CLVD}} = -\frac{M^*_{|\mathrm{min}|}}{|M^*_{|\mathrm{max}|}|}, \tag{7}$$

where $M^*_{|\mathrm{max}|}$ and $M^*_{|\mathrm{min}|}$ are the eigenvalues of deviatoric moment $\mathbf{M}^* = \mathbf{M}^{\mathrm{CLVD}} + \mathbf{M}^{\mathrm{DC}}$, with the maximum and minimum absolute values, respectively. To assess the relative amounts of the DC, CLVD, and ISO components in a moment tensor, we usually calculate their percentages as

$$\mathrm{ISO} = \frac{1}{3}\frac{\mathrm{Tr}(\mathbf{M})}{|M_{|\mathrm{max}|}|} \times 100, \tag{8}$$

$$\mathrm{CLVD} = 2\varepsilon^{\mathrm{CLVD}}(100 - |\mathrm{ISO}|), \tag{9}$$

$$\mathrm{DC} = 100 - |\mathrm{ISO}| - |\mathrm{CLVD}|, \tag{10}$$

where $M_{|\mathrm{max}|}$ denotes the eigenvalue of $\mathbf{M}$ with maximum absolute value.

MOMENT TENSORS IN ISOTROPIC MEDIA

The moment tensors are simplified considerably under the assumption of isotropy. Taking into account that the elastic parameters c_{ijkl} can be expressed by Lamé constants as (Aki and Richards, 2002, equation 2.33)

$$c_{ijkl} = \lambda\delta_{ij}\delta_{kl} + \mu(\delta_{ik}\delta_{jl} + \delta_{il}\delta_{jk}), \tag{11}$$

equation 1 yields

$$M_{ij} = \lambda D_{kk}\delta_{ij} + 2\mu D_{ij},$$

$$D_{kk} = D_{11} + D_{22} + D_{33} = uS\mathbf{n} \cdot \boldsymbol{\nu}, \tag{12}$$

where the dot is the scalar product. Moment tensor $\mathbf{M}$ is diagonalized as (Vavryčuk, 2005, equation 42)

$$\mathbf{M}^{\mathrm{diag}} = uS\begin{bmatrix} (\lambda + \mu)\mathbf{n} \cdot \boldsymbol{\nu} + \mu & 0 & 0 \\ 0 & \lambda\mathbf{n} \cdot \nu & 0 \\ 0 & 0 & (\lambda + \mu)\mathbf{n} \cdot \boldsymbol{\nu} - \mu \end{bmatrix} \tag{13}$$

in the coordinate system of the eigenvectors of $\mathbf{M}$,

$$\mathbf{e}_1 = \frac{\mathbf{n} + \boldsymbol{\nu}}{|\mathbf{n} + \boldsymbol{\nu}|}, \quad \mathbf{e}_2 = \frac{\mathbf{n} \otimes \boldsymbol{\nu}}{|\mathbf{n} \otimes \boldsymbol{\nu}|}, \quad \mathbf{e}_3 = \frac{\mathbf{n} - \boldsymbol{\nu}}{|\mathbf{n} - \boldsymbol{\nu}|}, \tag{14}$$

where $\otimes$ denotes the vector product. Assuming that the source is shear, then

$$\mathbf{n} \cdot \boldsymbol{\nu} = n_1\nu_1 + n_2\nu_2 + n_3\nu_3 = 0, \tag{15}$$

and equation 13 is simplified further to (Aki and Richards, 2002, p. 59)

$$\mathbf{M}^{\mathrm{diag}} = \mu uS\begin{bmatrix} +1 & 0 & 0 \\ 0 & 0 & 0 \\ 0 & 0 & -1 \end{bmatrix}, \tag{16}$$

which represents a pure DC source. Hence, shear faulting in isotropic media generates no CLVD or ISO components.

SHEAR FAULTING IN WEAK TRANSVERSE ISOTROPY

Thomsen's anisotropy parameters

Assuming a shear source situated in a weakly TI medium, the medium is described by the elastic parameters of the isotropic background C_{33} and C_{44}, and by Thomsen's anisotropy parameters (Thomsen, 1986; Tsvankin and Thomsen, 1994):

$$\varepsilon = \frac{C_{11} - C_{33}}{2C_{33}}, \tag{17}$$

$$\gamma = \frac{C_{66} - C_{44}}{2C_{44}}, \tag{18}$$

$$\sigma = \frac{1}{2C_{44}}\left[C_{11} - C_{44} - \frac{(C_{13} + C_{44})^2}{C_{33} - C_{44}}\right], \tag{19}$$

where C_{kl} are the elastic parameters in the Voigt notation. The elastic parameters are expressed in the coordinate system with the symmetry axis along the vertical. Thomsen's parameters ε, γ, and σ can serve as a measure of strength of TI; they are zero for isotropy and close to zero for weak anisotropy.

Moment tensors

Let us assume fixed geometry of faulting with fault normal $\mathbf{n} = (0,0,1)^T$ and slip direction $\boldsymbol{\nu} = (1,0,0)^T$. The symmetry axis of transverse isotropy is inclined, specified by unit direction vector $\mathbf{t}$.

Under weak anisotropy, the moment tensor $\mathbf{M}$ can be expressed as

the sum of the moment tensor $\mathbf{M}^0$ produced by shear faulting in the isotropic background and its perturbation $\Delta\mathbf{M}$ produced by anisotropy,

$$\mathbf{M} = \mathbf{M}^0 + \Delta\mathbf{M}, \tag{20}$$

where

$$\mathbf{M}^0 = \begin{bmatrix} 0 & 0 & M_0 \\ 0 & 0 & 0 \\ M_0 & 0 & 0 \end{bmatrix}, \quad \Delta\mathbf{M} = \begin{bmatrix} \Delta M_{11} & \Delta M_{12} & \Delta M_{13} \\ \Delta M_{12} & \Delta M_{22} & \Delta M_{23} \\ \Delta M_{13} & \Delta M_{23} & \Delta M_{33} \end{bmatrix}, \tag{21}$$

and M_0 denotes the scalar seismic moment, $M_0 = uSc_{44}$. The components of $\Delta\mathbf{M}$ are expressed in terms of Thomsen's anisotropy parameters as follows:

$$\Delta M_{11} = M_0 t_1 t_3 [-\kappa\varepsilon + \sigma(2t_1^2 - 1)],$$
$$\Delta M_{22} = M_0 t_1 t_3 [-\kappa\varepsilon + \sigma(2t_2^2 - 1) + 4\gamma],$$
$$\Delta M_{33} = M_0 t_1 t_3 [-\kappa\varepsilon + \sigma(2t_3^2 - 1)],$$
$$\Delta M_{12} = 2M_0 t_2 t_3 (-\gamma + \sigma t_1^2),$$
$$\Delta M_{13} = 2M_0 (\gamma t_2^2 + \sigma t_1^2 t_3^2),$$
$$\Delta M_{23} = 2M_0 t_1 t_2 (-\gamma + \sigma t_3^2), \tag{22}$$

where

$$\kappa = C_{33}/C_{44}. \tag{23}$$

The trace of the moment tensor reads

$$\mathrm{Tr}(\mathbf{M}) = \mathrm{Tr}(\Delta\mathbf{M}) = M_0 t_1 t_3 (-3\kappa\varepsilon + 4\gamma - \sigma); \tag{24}$$

hence, it is zero for isotropic media, but generally nonzero for TI. Using the formulas for calculating the perturbation of eigenvalues of $\mathbf{M}$ (Korn and Korn, 2000),

$$\Delta M_1 = \Delta M_{kl} e_{1k} e_{1l}, \quad \Delta M_2 = \Delta M_{kl} e_{2k} e_{2l},$$
$$\Delta M_3 = \Delta M_{kl} e_{3k} e_{3l}, \tag{25}$$

I obtain

$$\Delta M_1 = M_0 t_1 t_3 (-\kappa\varepsilon + 2\sigma t_1 t_3) + M_0 t_2^2 (2\gamma - \sigma t_1 t_3),$$
$$\Delta M_2 = M_0 t_1 t_3 [-\kappa\varepsilon + \sigma(2t_2^2 - 1) + 4\gamma],$$
$$\Delta M_3 = M_0 t_1 t_3 (-\kappa\varepsilon - 2\sigma t_1 t_3) - M_0 t_2^2 (2\gamma + \sigma t_1 t_3), \tag{26}$$

where vectors $\mathbf{e}_1$, $\mathbf{e}_2$, and $\mathbf{e}_3$ are the eigenvectors of moment tensor $\mathbf{M}^0$ referred to the isotropic background,

$$\mathbf{e}_1 = \frac{1}{\sqrt{2}}(1,0,1)^T, \quad \mathbf{e}_2 = (0,1,0)^T, \quad \mathbf{e}_3 = \frac{1}{\sqrt{2}}(-1,0,1)^T. \tag{27}$$

Note that ΔM_i is the perturbation of eigenvalue M_i of moment tensor $\mathbf{M}$, while ΔM_{ij} is the perturbation of moment tensor component M_{ij}.

Non-DC components

Assuming that perturbations ΔM_1, ΔM_2, and ΔM_3 are small with respect to M_0, $\mathrm{Tr}(\mathbf{M})$ and $M_{|\mathrm{min}|}^*$, expressed as

$$\mathrm{Tr}(\mathbf{M}) = \Delta M_1 + \Delta M_2 + \Delta M_3,$$
$$M_{|\mathrm{min}|}^* = \Delta M_2 - \frac{1}{3}\mathrm{Tr}(\mathbf{M}) = -\frac{1}{3}(\Delta M_1 + \Delta M_3 - 2\Delta M_2), \tag{28}$$

are also small, and $M_{|\mathrm{max}|}$ and $M_{|\mathrm{max}|}^*$, expressed as

$$|M_{|\mathrm{max}|}| = \max(M_0 + \Delta M_1, M_0 - \Delta M_3), \tag{29}$$

$$|M_{|\mathrm{max}|}^*| = \max\left(M_0 - \frac{1}{3}[\Delta M_2 + \Delta M_3 - 2\Delta M_1], \right.$$
$$\left. M_0 + \frac{1}{3}[\Delta M_1 + \Delta M_2 - 2\Delta M_3]\right), \tag{30}$$

are close to M_0. Hence, considering first-order perturbations, I substitute $|M_{|\mathrm{max}|}|$ and $|M_{|\mathrm{max}|}^*|$ in equations 7 and 8 simply by M_0 and obtain

$$\mathrm{ISO} \cong 100 \times \frac{\Delta M_1 + \Delta M_2 + \Delta M_3}{3M_0}, \tag{31}$$

$$\varepsilon^{\mathrm{CLVD}} \cong \frac{\Delta M_1 + \Delta M_3 - 2\Delta M_2}{3M_0}, \tag{32}$$

where, again, ISO is expressed as a percentage. Substituting equations 26 into equations 31 and 32, I finally obtain

$$\mathrm{ISO} \cong 100 \times \frac{1}{3} t_1 t_3 (-3\kappa\varepsilon + 4\gamma - \sigma), \tag{33}$$

$$\varepsilon^{\mathrm{CLVD}} \cong \frac{2}{3} t_1 t_3 [-4\gamma + \sigma(1 - 3t_2^2)]. \tag{34}$$

The CLVD is obtained by inserting equations 33 and 34 into equation 9.

More accurate equations than 33 and 34 can be derived if $|M_{|\mathrm{max}|}|$ and $|M_{|\mathrm{max}|}^*|$ are calculated correctly by equations 28 and 29, rather than replaced by M_0. This approach yields

$$\mathrm{ISO} \cong 100 \times \frac{1}{3D_1} t_1 t_3 (-3\kappa\varepsilon + 4\gamma - \sigma), \tag{35}$$

$$\varepsilon^{\mathrm{CLVD}} \cong \frac{2}{3D_2} t_1 t_3 [-4\gamma + \sigma(1 - 3t_2^2)], \tag{36}$$

where

$$D_1 = \max(1 + t_1 t_3 [\mp\kappa\varepsilon + 2\sigma t_1 t_3] + t_2^2 [2\gamma \mp \sigma t_1 t_3]),$$

$$D_2 = \max\left(1 + \frac{2}{3}\gamma[3t_2^2 \mp 2t_1t_3]\right.$$
$$\left. + \frac{1}{3}\sigma t_1 t_3[6t_1t_3 \mp 3t_2^2 \pm 1]\right), \qquad (37)$$

and I have used the following notation: $\max(a \pm b \mp c) = \max(a + b - c, a - b + c)$.

I derived the non-DC components of **M** assuming a fixed geometry of faulting with fault normal $\mathbf{n} = (0,0,1)^T$ and slip direction $\boldsymbol{\nu} = (1,0,0)^T$. General formulas valid for shear faulting with arbitrarily oriented fault normal **n** and slip direction $\boldsymbol{\nu}$ are obtained from the formulas derived here by applying the following substitutions:

$$t_1 = \mathbf{t} \cdot \boldsymbol{\nu}, \quad t_3 = \mathbf{t} \cdot \mathbf{n}, \quad \text{and} \quad t_2^2 = 1 - t_1^2 - t_3^2, \quad (38)$$

where **t** is the direction of the symmetry axis.

APPLICATION TO CRUSTAL ROCKS

In this section, I apply the derived formulas to theoretical models of crustal anisotropy and to anisotropy observed on crustal rock samples. Four anisotropy models are considered: one model produced by the presence of aligned water-filled cracks and three models produced by layering. The effective anisotropy is calculated using the Hudson (1981) theory for cracks and the Backus (1962) averaging for layers. Furthermore, I consider ten published models of anisotropy observed in rocks. The anisotropy was measured in the laboratory for sedimentary and metamorphic rock samples that originated in the upper crust. The presented models clearly do not cover all possible variations of anisotropy in focal areas, but they do provide insight into how significant non-DC components can be generated by shear faulting in the crust and the accuracy of the derived approximations for calculating non-DC components.

The anisotropy models are summarized in Table 1. The table lists Thomsen's anisotropy parameters for each model, together with the rock sample or model identification and the literature reference. Because some of the models were defined in terms of standard elastic parameters (Shearer and Chapman, 1989; Baptie et al., 1995; Rabbel et al., 2004; Godfrey et al., 2000), the anisotropy parameters in the table had to be calculated using equations 17–19. Table 2 summarizes the anisotropy strength of P-, SV-, and SH-waves, and maximum absolute values of the CLVD and ISO components generated by shear faulting in the specified anisotropy model. The percentage anisotropy strength is defined as

Table 1. Anisotropy models — ν^P and ν^S are vertical P and S velocities; ε, γ, and δ are Thomsen's anisotropy parameters; ρ is density.

Model/rock	ν^P (km/s)	ν^S (km/s)	ε	γ	δ	ρ (g/cm^3)	Model/rock identification	Reference
					Theoretical models			
Cracks	4.477	2.258	0.005	0.125	−0.111	2.80	Model 1	Shearer and Chapman (1989)
Layers I	3.907	2.185	0.021	0.015	0.008	2.60	PTL1	Baptie et al. (1995, Table 1)
Layers II	3.091	1.749	0.150	0.141	0.023	2.60	PTL2	Baptie et al. (1995, Table 1)
Layers III	2.585	1.472	0.323	0.318	0.032	2.60	PTL3	Baptie et al. (1995, Table 1)
					Rocks			
Sandstone I	4.476	2.814	0.097	0.051	0.091	2.50	Mesaverde (4912) immature sandstone	Thomsen (1986, Table 1)
Sandstone II	4.099	2.346	0.077	0.066	0.010	2.45	Mesaverde (4946) immature sandstone	Thomsen (1986, Table 1)
Sandstone III	4.349	2.571	0.091	0.105	0.148	2.46	Mesaverde (5481.3) immature sandstone	Thomsen (1986, Table 1)
Shale I	3.901	2.682	0.137	0.026	−0.012	2.64	Mesaverde shale (1599)	Thomsen (1986, Table 1)
Shale II	4.721	2.890	0.135	0.180	0.205	2.64	Cotton Valley shale	Thomsen (1986, Table 1)
Shale III	2.202	0.969	0.015	0.030	0.060	2.25	Pierre shale (z = 950 m)	Thomsen (1986, Table 1)
Gneiss I	6.000	3.380	0.043	0.125	−0.007	2.78	KTB (2.2–3.0 km)	Rabbel et al. (2004, Table 1)
Gneiss II	5.109	3.126	0.215	0.222	0.107	2.75	KTB (7.9–8.2 km)	Rabbel et al. (2004, Table 1)
Phyllite	5.947	3.438	0.100	0.149	−0.043	2.72	Chugach phyllite, TA-2, p = 100 MPa	Godfrey et al. (2000, Table 1)
Schist	5.727	3.439	0.150	0.049	0.085	2.72	Pelona schist, LA-1, p = 100 MPa	Godfrey et al. (2000, Table 1)

$$a = 200 \times \frac{c^{\max} - c^{\min}}{c^{\max} + c^{\min}}, \qquad (39)$$

where $c^{\max}$ and $c^{\min}$ are the maximum and minimum phase velocities of the given wave type. The maximum values of the CLVD and ISO were calculated under fixed geometry of faulting and over all orientations of the symmetry axis. The direction of the symmetry axis varied in a grid of spherical angles θ and φ in steps of 2°. The CLVD and ISO were calculated using exact equations 8 and 9 and approxi-

mate equations 33–36. The CLVD and ISO calculated using equations 33 and 34 are denoted as CLVD$_1$ and ISO$_1$, and those calculated using equations 35 and 36 are denoted as CLVD$_2$ and ISO$_2$.

The directional variation of phase velocity as a function of the wave normal (i.e., the normal to the wavefront of a propagating plane wave) is exemplified for the Layers II model (see Table 1) in Figures 1 and 2. The anisotropy strength is 13.1%, 8.1%, and 12.4% for the P-, SV-, and SH-waves, respectively (see Table 2). Shear faulting in this anisotropy generates the maximum ISO and CLVD components of 14.4% and 18.7%. The directional variation of the

Table 2. Anisotropy strength and percentages of ISO and CLVD. Quantities a^P, a^{SV} and a^{SH} denote the anisotropy strength of P-, SV-, and SH-waves, which is defined in equation 39. ISO^{max} and CLVD^{max} are the exact maximum absolute values of the ISO and CLVD components. ISO$_1^{max}$ and CLVD$_1^{max}$ are the approximate values calculated using equations 33 and 34, and ISO$_2^{max}$ and CLVD$_2^{max}$ are approximate values calculated using equations 35 and 36.

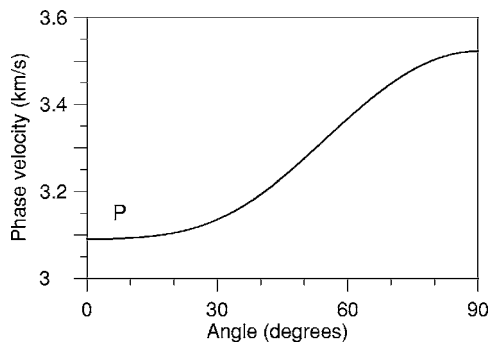| Model/rock	a^P (%)	a^{SV} (%)	a^{SH} (%)	ISO^{max} (%)	ISO$_1^{max}$ (%)	ISO$_2^{max}$ (%)	CLVD^{max} (%)	CLVD$_1^{max}$ (%)	CLVD$_2^{max}$ (%)
				Theoretical models					
Cracks	3.5	11.0	11.2	0.6	0.1	0.1	19.9	24.3	19.6
Layers I	2.1	1.0	1.5	2.9	3.1	2.9	2.6	2.6	2.6
Layers II	13.1	8.1	12.4	14.4	20.6	14.4	18.7	22.8	18.8
Layers III	24.8	15.2	24.5	22.4	43.5	22.4	31.7	44.9	32.2
				Rocks					
Sandstone I	8.9	0.3	4.9	8.2	9.1	8.1	10.2	11.4	11.1
Sandstone II	7.2	4.6	6.2	8.8	10.8	8.8	10.4	11.6	10.4
Sandstone III	8.4	3.6	9.5	3.7	3.3	3.1	33.9	37.6	37.0
Shale I	12.1	6.6	2.5	13.8	18.0	13.8	10.2	11.5	10.2
Shale II	11.9	3.9	15.3	3.6	2.9	2.7	49.8	58.7	55.6
Shale III	1.9	5.9	2.9	2.0	2.0	2.2	23.6	23.0	24.4
Gneiss I	4.1	3.6	11.2	0.8	0.9	0.8	20.3	23.4	20.4
Gneiss II	17.9	5.5	18.3	13.3	18.8	13.1	27.5	35.1	28.8
Phyllite	9.5	9.3	13.0	9.0	12.2	8.9	20.4	25.5	20.5
Schist	13.1	3.7	4.7	15.9	20.6	15.9	8.2	8.6	8.0

Figure 1. Phase velocity of the P-wave as a function of the angle between the wave normal and the symmetry axis for the Layers II model.
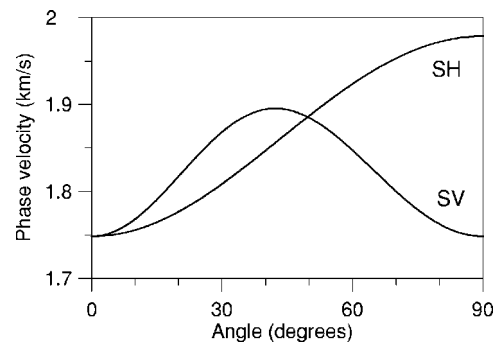

Figure 2. Phase velocity of the SV- and SH-waves as a function of the angle between the wave normal and the symmetry axis for the Layers II model.

exact values of the ISO and CLVD together with errors produced by approximate equations 33–36 are shown in Figures 3 and 4. The errors are the difference between the approximate and exact percentages. The errors are almost 6% and 4% for the ISO_1 and $CLVD_1$. The ISO_2 and $CLVD_2$ are more accurate, having maximum errors of 0.04% and 0.8%.

Figure 3a shows that the exact ISO component for Layers II has one maximum and one minimum that lie in the plane of the slip and fault normal. The same or a similar pattern can be observed also for the other anisotropy models (see Figure 5). However, the directional variation of the CLVD percentage is more variable for the different anisotropy models, and can be more complicated. In the Layers II model, the CLVD displays two maxima and two minima that lie off

the plane defined by the slip and fault normal (see Figure 4a), but other models can produce a lower or higher number of local maxima and minima (see Figure 6).

The anisotropy models presented in Tables 1 and 2 span the range of anisotropy strength from 2% to almost 25%. Shear faulting in the models produces the maximum ISO percentage in the range from 0.6% to 22.4% and the maximum CLVD percentage from 2.6% to 49.8%. Usually, the CLVD is higher than the ISO, but for some models (Shale I, Schist) the opposite is observed. Interestingly, some models with a rather weak anisotropy generate a considerably high CLVD. This applies, for example, to Shale III of anisotropy strength less than 6% that generates a CLVD of 23.6%, and to Sandstone III of anisotropy strength less than 10%, but with a CLVD of 33.9%. This implies that shear faulting in crustal rocks can generate detectable and significant non-DC components owing to anisotropy.

Figure 3. The ISO components generated by shear faulting in the Layers II model with an inclined symmetry axis: (a) the exact ISO, (b) the difference between the ISO_1 and the exact ISO, and (c) the difference between the ISO_2 and the exact ISO. The geometry of faulting is fixed; the fault normal is along the z-axis, and the slip direction is along the x-axis. Points inside the circle correspond to TI with a varied orientation of the symmetry axis. The plus sign marks the TI with the vertical symmetry axis; the points along the circle correspond to the TI with horizontal symmetry axes. Equal-area projection is used.

Figure 5. The percentage of the exact ISO components generated by shear faulting in the (a) Sandstone III model, (b) Sandstone II model, and (c) Shale I model. For details of the faulting geometry and the projection, see the caption of Figure 3.
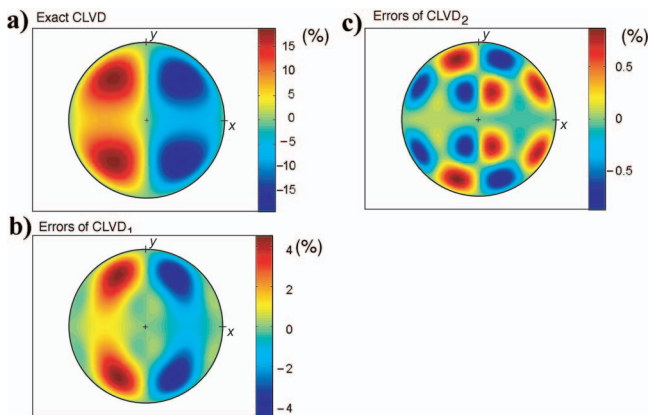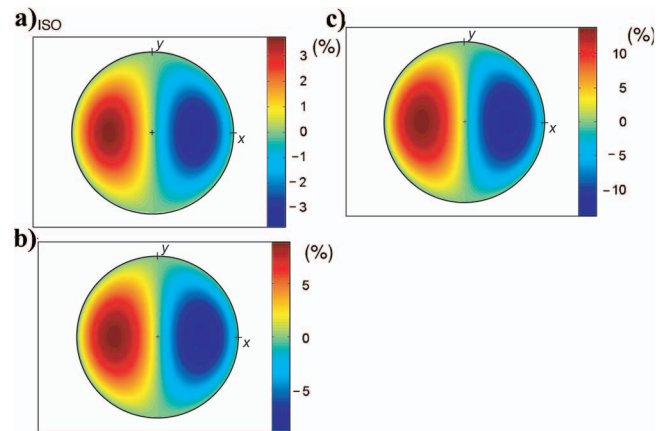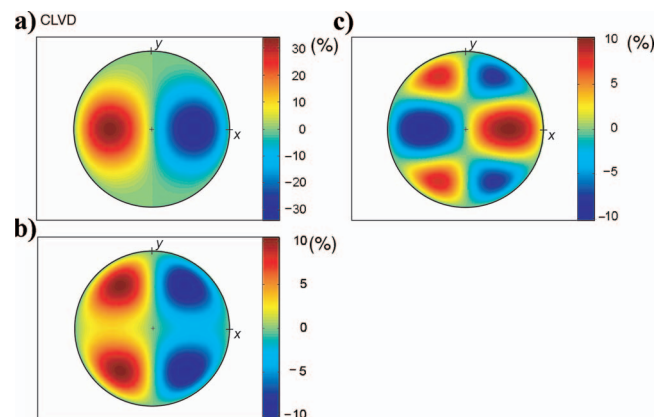

Figure 4. The CLVD components generated by shear faulting in the Layers II model with an inclined symmetry axis: (a) the exact CLVD, (b) the difference between the $CLVD_1$ and the exact CLVD, and (c) the difference between the $CLVD_2$ and the exact CLVD. For details, see the caption of Figure 3.

Figure 6. The percentage of the exact CLVD components generated by shear faulting in the (a) Sandstone III model, (b) Sandstone II model, and (c) Shale I model. For details of the faulting geometry and the projection, see the caption of Figure 3.

CONCLUSIONS

Shear faulting in anisotropic rocks produces non-DC mechanisms. For weak anisotropy, the formulas for the percentages of the CLVD and ISO can be simplified using first-order perturbation theory. For weak TI, the CLVD and ISO can be expressed using Thomsen's anisotropy parameters. If we fix the fault normal and slip direction and vary the orientation of the symmetry axis, the ISO component has an identical directional variation for all values of anisotropy parameters. It is characterized by one maximum and one minimum generated if the symmetry axis lies in the plane of the fault normal and slip and is inclined by 45° from the fault normal. The directional variation of the CLVD is more dependent on anisotropy parameters and can be more complicated. The maxima and minima can lie off the plane of the fault normal and slip. Usually, the CLVD is larger than the ISO and can attain values up to 30%–35% for anisotropy with strength of 10% or less. Hence, the anisotropy of rocks can influence significantly computed focal mechanisms and should thus be considered in their interpretations.

The interpretations, however, should also consider origins of non-DC mechanisms other than anisotropy, such as numerical error in the moment tensor inversion, faulting on nonplanar fractures, and tensile faulting produced by opening or closing of fractures. Separating the contribution of anisotropy from those of the other origins of the non-DC mechanisms can be complicated and ambiguous. Nevertheless, in cases when it is possible, the non-DC mechanisms can be exploited for estimating the geometry of faulting and the anisotropy in the source area.

ACKNOWLEDGMENTS

REFERENCES

Aki, K., and P. G. Richards, 2002, Quantitative seismology: University Science Books.
Babuška, V., and M. Cara, 1991, Seismic anisotropy in the earth: Kluwer Academic Publisher.
Backus, G. E., 1962, Long-wave anisotropy produced by horizontal layering: Journal of Geophysical Research, **66**, 4427–4440.
Baptie, B., S. Crampin, and E. Liu, 1995, Displaying shear-wave splitting in cross-hole surveys for materials with combinations of EDA and PTL anisotropies: Canadian Journal of Exploration Geophysics, **29**, 227–235.
Červený, V., 2001, Seismic ray theory: Cambridge University Press.
Farra, V., 2004, Improved first-order approximation of group velocities in weakly anisotropic media: Studia Geophysica et Geodaetica, **48**, 199–213.
Farra, V., 2005, First-order ray tracing for qS waves in inhomogeneous weakly anisotropic media: Geophysical Journal International, **161**, 309–324, doi: 10.1111/j.1365-246X.2005.02570.x.
Godfrey, N. J., N. I. Christensen, and D. A. Okaya, 2000, Anisotropy of schists: Contribution of crustal anisotropy to active source seismic experiments and shear wave splitting observations: Journal of Geophysical Research, **105**, 27.991–28.007.
Helbig, K., 1994, Foundations of anisotropy for exploration seismics: Pergamon Press.
Hudson, J. A., 1981, Wave speeds and attenuation of elastic waves in material containing cracks: Geophysical Journal of Royal Astronomical Society, **64**, 133–150.
Jost, M. L., and R. B. Hermann, 1989, A student's guide to and review of moment tensors: Seismological Research Letters, **60**, 37–57.
Julian, B. R., A. D. Miller, and G. R. Foulger, 1998, Non-double-couple earthquakes, 1. Theory: Reviews of Geophysics, **36**, 525–549.
Kawasaki, I., and T. Tanimoto, 1981, Radiation patterns of body waves due to the seismic dislocation occurring in an anisotropic source medium: Bulletin of Seismological Society of America, **71**, 37–50.
Korn, G. A., and T. M. Korn, 2000, Mathematical handbook for scientists and engineers: Dover Publications.
Kravtsov, Y. A., and Y. I. Orlov, 1990, Geometrical optics of inhomogeneous media: Springer-Verlag.
Maxwell, S. C., and T. I. Urbancic, 2001, The role of passive microseismic monitoring in the instrumented oil field: The Leading Edge, **20**, 636–640.
Musgrave, M. J. P., 1970, Crystal acoustics: Holden-Day.
Pšenčík, I., and J. A. Dellinger, 2001, Quasi-shear waves in inhomogeneous weakly anisotropic media by the quasi-isotropic approach: A model study: Geophysics, **66**, 308–319.
Pšenčík, I., and D. Gajewski, 1998, Polarization, phase velocity, and NMO velocity of qP-waves in arbitrary weakly anisotropic media: Geophysics, **63**, 1754–1766.
Rabbel, W., et al., 2004, Superdeep vertical seismic profiling at the KTB deep drill hole (Germany): Seismic close-up view of a major thrust zone down to 8.5 km depth: Journal of Geophysical Research, **109**, B09309, doi: 10.1029/2004JB002975.
Rössler, D., G. Rümpker, and F. Krüger, 2004, Ambiguous moment tensors and radiation patterns in anisotropic media with applications to the modeling of earthquake mechanisms in W-Bohemia: Studia Geophysica et Geodaetica, **48**, 233–250.
Rutledge, J. T., and W. S. Phillips, 2003, Hydraulic stimulation of natural fractures as revealed by induced microearthquakes, Carthage Cotton Valley gas field, East Texas: Geophysics, **68**, 441–452.
Rutledge, J. T., W. S. Phillips, and B. K. Schuessler, 1998, Reservoir characterization using oil-production-induced microseismicity, Clinton County, Kentucky: Tectonophysics, **289**, 129–152.
Shearer, P. M., and C. H. Chapman, 1989, Ray tracing in azimuthally anisotropic media—I. Results for models of aligned cracks in the upper crust: Geophysical Journal International, **96**, 51–64.
Šílený, J., and V. Vavryčuk, 2002, Can unbiased source be retrieved from anisotropic waveforms by using an isotropic model of the medium?: Tectonophysics, **356**, 125–138.
Thomsen, L., 1986, Weak elastic anisotropy: Geophysics, **51**, 1954–1966.
Tsvankin, I., 2001, Seismic signatures and analysis of reflection data in anisotropic media: Pergamon Press.
Tsvankin, I., and L. Thomsen, 1994, Nonhyperbolic reflection moveout in anisotropic media: Geophysics, **59**, 1290–1304.
Vavryčuk, V., 2001, Inversion for parameters of tensile earthquakes: Journal of Geophysical Research, **106**, 16.339–16.355.
———, 2002, Non-double-couple earthquakes of January 1997 in West Bohemia, Czech Republic: Evidence of tensile faulting: Geophysical Journal International, **149**, 364–373.
———, 2004, Inversion for anisotropy from non-double-couple components of moment tensors: Journal of Geophysical Research, **109**, B07306, doi: 10.1029/2003JB002926.
———, 2005, Focal mechanisms in anisotropic media: Geophysical Journal International, **161**, 334–346, doi: 10.1111/j.1365-246X.2005.02585.x.
Vavryčuk, V., and I. Pšenčík, 1998, *PP* wave reflection coefficients in weakly anisotropic elastic media: Geophysics, **63**, 2129–2141.